Journal of Materials Chemistry A

Accepted Manuscript

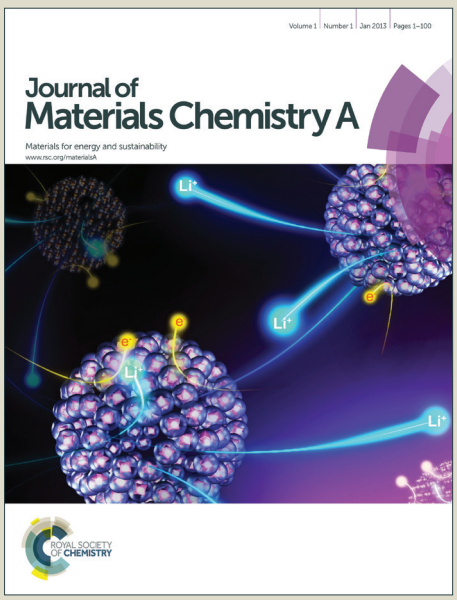

ROYAL SOCIETY OF CHEMISTRY

www.rsc.org/materialsA

Journal Name

ARTICLE

Demonstration of phonon-glass electron-crystal strategy in (Hf,Zr)NiSn half-Heusler thermoelectric materials by alloying

Received 00th January 20xx,
Accepted 00th January 20xx

DOI: 10.1039/x0xx00000x

www.rsc.org/

Yintu Liu,[a] Hanhui Xie,[a] Chenguang Fu,[a] G. Jeffrey Snyder,*[b] Xinbing Zhao[a] and Tiejun Zhu*[a]

The general phonon-glass electron-crystal strategy is to disrupt phonon transport without affecting electron transport. Disruption of phonon thermal conductivity by alloying and nanostructuring is well known but direct comparison of the scattering strength for electrons to that for phonons from disorder has not been made. Here we show that point defect disorder of Zr/Hf atoms in *M*NiSn (*M* = Hf, Zr, Ti) half-Heusler alloys effectively reduces lattice thermal conductivity as predicted from point defect scattering. However the introduced local atomic disorder produces negligible effect on the electron scattering process and the conduction band structure. The electron scattering potential observed on the conduction band electrons is less than 0.1 eV, ten times less than the typically observed. This phenomenon can be understood from the existence of intrinsic disorder in *M*NiSn system causing distinct mass and strain difference that effectively screens the effect of the induced disorder of Hf/Zr. The highest zT = 1.1 was obtained for $Zr_{0.2}Hf_{0.8}NiSn_{0.985}Sb_{0.015}$ at 1000 K. This results is a substantial improvement in zT due to alloying on the Zr/Hf site and demonstrated a dramatic improvement in TE performance that doesn't require nanoscale microstructures to avoid scattering of charge carriers.

Introduction

Energy recovery from waste heat at elevated temperatures is attracting more and more interest due to the increased demand for higher fuel efficiency and smaller environmental impact. Thermoelectric (TE) materials, which offer the possibility of directly converting waste heat into usable electricity, could be an important part of the solution to today's energy crisis.[1] The efficiency of a TE material is represented by the dimensionless figure of merit $zT = S^2\sigma T/\kappa$, where S is the Seebeck coefficient, σ is the electrical conductivity, T is the operating temperature and κ is the total thermal conductivity arising from two prime contributions, namely, the lattice part κ_L and the electronic part κ_e.

The optimal zT of thermoelectrics is essentially determined by the TE quality factor $B \propto \mu m^{*3/2}/\kappa_L$,[2] which is proportional to the density-of-states (DOS) effective mass m^*, the carrier mobility μ, and the reciprocal lattice thermal conductivity κ_L. The mobility is sensitive to the effective mass and scattering mechanisms. While a large m^* is favorable for high S, it will possibly lead to a significant reduction in mobility via $\mu \propto m^{*-5/2}$.[3] The general phonon-glass electron-crystal (PGEC) strategy for enhancing zT is to disrupt phonon transport to reduce κ_L without the deterioration of electron transport properties.[4] Disruption of phonon thermal conductivity by alloying[5,6] and nanostructuring[7,8] is well known but direct comparison of the scattering strength for electrons to that for phonons from disorder has not been made.

Half-Heusler (HH) alloys, with a valence electron count of 18, have been extensively studied as potential high temperature TE materials due to their narrow band gap and sharp slope of the density of states near the Fermi level.[9-12] The half-Heusler compounds of the general formula *M*NiSn (*M* = Ti, Hf, Zr) have been of significant interest for their high power factors ($S^2\sigma$) due to a combination of large Seebeck coefficient S and reasonably high electrical conductivity σ. A low deformation potential E_{def}, characterizing the weak coupling between phonons and electrons, was found to be beneficial for maintaining a relatively high electron mobility despite of the large DOS effective mass (m^* = 2.8±0.2 m_e) for *M*NiSn based alloys.[13,14] To optimize the electrical performance of this system, many efforts have been devoted to tune the Fermi level by doping Sb on the Sn sites,[15,16] or controlling the atomic disorder.[17] An optimal carrier concentration n = 3~4 × 10^{20} cm^{-3} has been demonstrated in the Sb doped ZrNiSn compounds with peak zT = 0.8 at 873 K.[14]

However, the high thermal conductivity hinders the commercial application of HH alloys. The nanostructuring strategy,[18] initially inspired by the idea of utilizing quantum size effects, was adopted in HH system to enhance phonon scattering at the grain boundaries and reduce the lattice thermal conductivity.[16,19-22] The refined grain sizes, however, will also cause the deterioration in carrier mobility and offset the gain from the reduction of κ_L. The mean free path of carriers and phonons for *M*NiSn system was reported to be of the same order (~ 10^{-9} m) at room temperature and the zT

[a] State Key Laboratory of Silicon Materials and School of Materials Science and Engineering, Zhejiang University, Hangzhou 310027, China. E-mail: zhutj@zju.edu.cn
[b] Department of Materials Science and Engineering, Northwestern University, Evanston, IL 60208, USA. E-mail: jeff.snyder@northwestern.edu

enhancement based on grain refinement is quite limited.[23] The effectiveness of isoelectronic alloying on the *M* or Ni sublattice in causing additional mass or strain fluctuation to reduce κ_L was successfully demonstrated.[15,24] A peak zT ~ 1.0 has been attained in these compounds.[16,24]

The isoelectronic substitution of Hf at the Zr site is a routine scheme for suppressing κ_L.[15,16,24] However, there are few reports on the influences of Hf substitution on the electron transport and the optimal Hf content is still ambiguous.[16, 24] In this work, we study the *n*-type $Zr_{1-x}Hf_xNiSn$ (x = 0-1) solid solutions throughout the composition range, which is an ideal system for quantitative study of the influences of isoelectronic alloying on TE transport. The experimental electrical and thermal properties are analyzed by the single Kane band (SKB) model[25] and the Callaway model.[26,27] The atomic disorder of Zr/Hf sites in HH alloys effectively reduces lattice thermal conductivity as predicted from enhanced point defect scattering. However, the introduced atomic disorder almost has no effect on electron transport. A highest zT = 1.1 was obtained for $Zr_{0.2}Hf_{0.8}NiSn_{0.985}Sb_{0.015}$ at 1000 K. This result is an effective demonstration of PGEC strategy in HH compounds by simple alloying, other than nanostructuring, to avoid the deterioration of carrier transport properties.

Experimental

The samples were fabricated by a time-efficient method combining levitation melting and spark plasma sintering (SPS).[16] Alloys with nominal composition $Zr_{1-x}(Hf)_xNiSn_{0.985}Sb_{0.015}$ (x = 0, 0.2, 0.4, 0.5, 0.6, 0.8, 1.0) were first prepared by levitation melting of stoichiometric amounts of Zr (piece, 99.99%), Ni (block, 99.99%), Sn (particles, 99.99%), and Sb (block, 99.99%) under an argon atmosphere for 2 min, and the melt was quenched in a water-cooled copper crucible. The ingots were remelted twice to ensure homogeneity. Mechanical milling was carried out with oscillation frequency 20 MHz for 20 min. The powders were then sintered by SPS (SPS-1050, Sumitomo Coal Mining Co.) at 1175 K under 65 MPa in vacuum for 10 min. The as-sintered samples, of which the relative density was found to be ~ 95%, were used for measurements of thermal conductivity and Hall data, and then cut into rectangular bars for Seebeck coefficient measurement.

The phase structure of the powders and sintered samples were studied by X-ray diffraction (XRD) on a RigakuD/MAX-2550PC diffractometer using Cu K_α radiation (λ = 1.5406 Å) and the chemical composition was obtained during electron probe microanalysis (EPMA, JOEL, JXA-8100) using wavelength dispersive spectroscopy (WDS).

The electrical transport was characterized via Hall effect, electrical conductivity, and Seebeck coefficient measurements. The in-plane electrical resistivities and Hall coefficients were measured using the Van der Pauw method in a magnetic field up to ±2 T.[28] The Hall carrier concentration n_H is calculated via $n_H = 1/eR_H$, where R_H is the Hall coefficient and e is the electron charge The Hall mobility μ_H is calculated from the Hall coefficient and electrical conductivity $\mu_H = R_H\sigma$. The electrical conductivity and Seebeck coefficient from 300-1100 K were measured on a commercial Linseis LSR-3 system using a DC four-probe method and differential voltage/temperature technique, respectively. The thermal conductivity, κ, was calculated by using $\kappa = D\rho C_p$, where ρ is the sample density estimated by an Archimedes' method. The thermal diffusivity D, and specific heat C_p, were measured by a laser flash method on Netzsch LFA457 instrument with a Pyroceram standard.

Normal and shear ultrasonic measurements are performed at room temperature using input from a Panametrics 5052 pulser/receiver with the filter at 0.03 MHz. The response is recorded via a Tektronic TDS5054B-NV digital oscilloscope.

Results and discussion

The powder XRD patterns in Fig. 1(a) taken on the levitation-melted ingots of $Zr_{1-x}Hf_xNiSn_{0.985}Sb_{0.015}$ (x = 0-1) could be well indexed to the cubic MgAgAs-type crystal structure, and no secondary phases were identified. Fig. 1(b) shows the Hall carrier concentration n_H and Seebeck coefficient S as a function of Hf content. The measured $n_H = 4\times10^{20}$ cm^{-3} at 300 K is around the optimal carrier concentration of the *M*NiSn system.[14] The small random fluctuations in n_H and S assure that the following discussions are based on the almost unchanged carrier concentration and band structure almost regardless of Hf substitution.

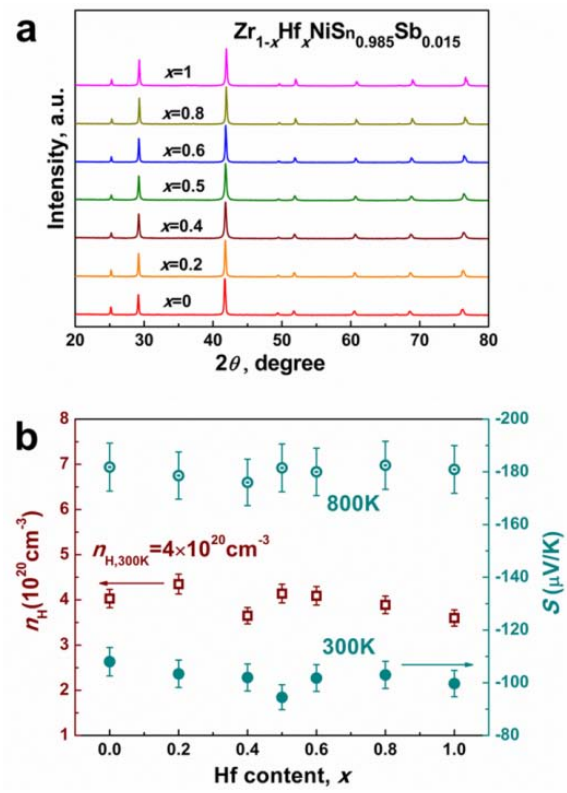

Fig.1 (a) XRD patterns of the $Zr_{1-x}Hf_xNiSn_{0.985}Sb_{0.015}$ samples with no impurities observed.(b) Hall carrier density (300 K) and Seebeck coefficient (300 K and 800 K) as a function of Hf content for $Zr_{1-x}Hf_xNiSn_{0.985}Sb_{0.015}$ (x = 0 - 1).

The conduction bands of both ZrNiSn and HfNiSn contain a single minimum at *X* point in the first Brillouin zone.[29-31] The dispersion relation near the band edge can be explained well by the non-parabolic Kane band model.[14] Theoretical calculation and experimental analysis both gave similar DOS effective mass m^* = (2.8±0.2) m_e for ZrNiSn system.[13,15,32] As for HfNiSn system, a relatively smaller m^* and higher Hall mobility μ_H were found experimentally.[23,33] In this work, the effective mass was performed by both single parabolic band (SPB) model and single kane band (SKB) model (see Fig. 2(a)), and no obvious difference but a weak decreasing trend of m^* from ZrNiSn to HfNiSn was observed. Considering the uncertainty in the carrier concentration and Seebeck coefficient measurements, this weak decrease in the effective mass deserves further investigation.

In most cases, an additional scattering mechanism will take actions in solid solutions due to the random distribution of different atoms on the same lattice site. The mobility in TE solid solutions is thus lower than that of pure compound.[6,34,35] It is noticeable and interesting, however, that no deterioration of carrier mobility was observed in the HH alloys with the Hf substitution at Zr site through the whole composition range, as shown in Fig. 2(b), different from most of typical TE materials with alloying.

Fig. 2(c) shows all the samples roughly have the similar mobility magnitude and temperature dependence. The electrical resistivity of alloys or intermetallic compounds, normally saturates when the charge mean free path becomes comparable to the interatomic spacing, which gives a minimum value to the carrier mobility and is called as the Ioffe-Regel rule. Such phenomenon was observed in some TE systems with extremely low carrier mobility, for instance, the TAGS-85.[36] The calculated Ioffe-Regel limit of carrier mobility for the HH system is far below the measured mobility, as shown in Fig. 2(c), indicating that the non-deteriorated mobility with alloying is not due to the reach of Ioffe-Regel limit.

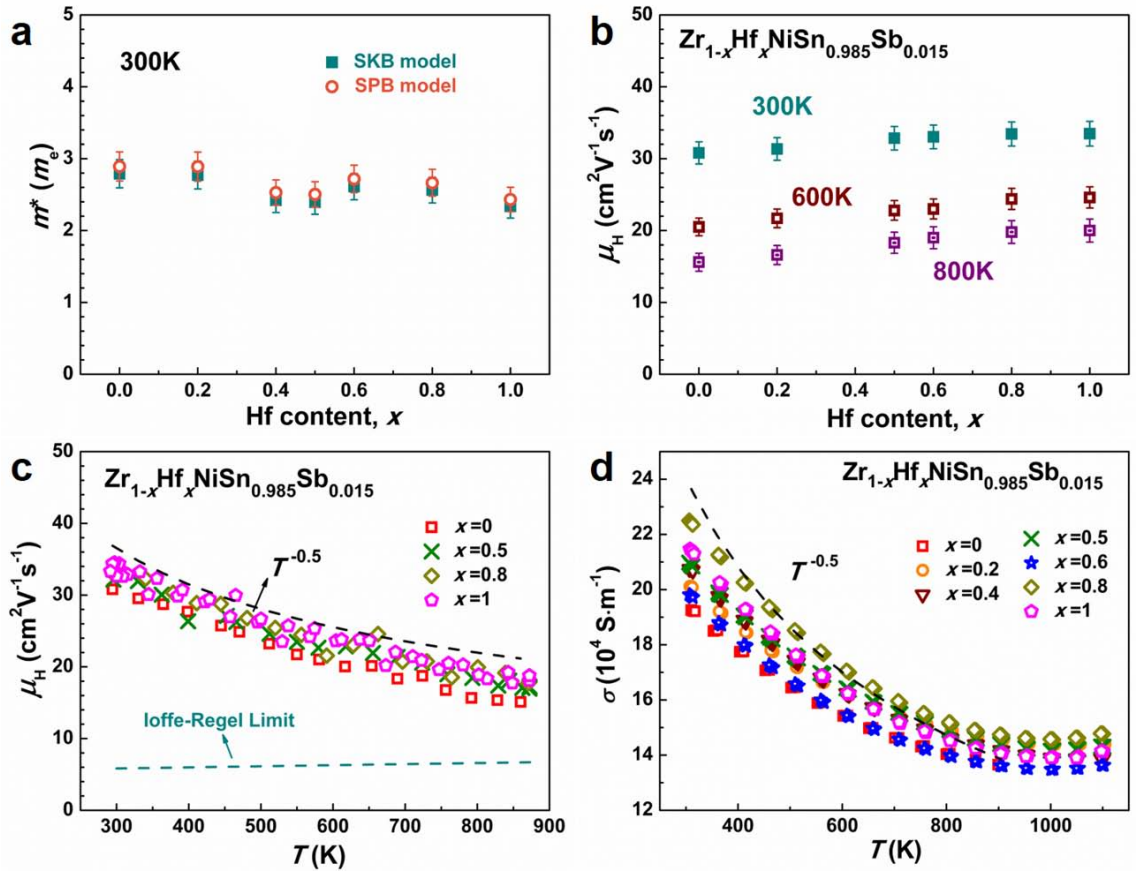

Fig.2 (a) DOS effective mass as a function of Hf content at 300 K. (b) Hall mobility μ_H as a function of Hf content at 300 K, 600 K and 800 K. (c) Temperature dependence of Hall mobility μ_H. (d) Temperature dependence of electrical conductivity for $Zr_{1-x}Hf_xNiSn_{0.985}Sb_{0.015}$.

A typical alloy scattering behavior $\mu_H \sim T^{-0.5}$ was observed for all the $Zr_{1-x}Hf_xNiSn_{0.985}Sb_{0.015}$ samples, consistent with the temperature dependence of electrical conductivity (Fig. 2(d)), indicating the existence of strong alloy disorder. An extremely low alloy scattering potential E_{al} ~ 0.1 eV was derived for the Hf substituted alloys by SKB model, which is about ten time less than the typically observed.[13] The local atomic disorder produces negligible effect on the electron scattering process. This phenomenon can be understood from the existence of intrinsic Ni-interstitial atomic disorder in this system,[37-40] which has the much higher alloy scattering potential that effectively screens the additional disorder on the Zr/Hf sites. The Ni-interstitial site disorder in *M*NiSn system causes distinct contrast of mass and strain differences compared to the Zr/Hf

disorder.[14,37] A typical alloy scattering dominated charge transport with $\mu_H \sim T^{-0.5}$ relationship is also observed for ternary ZrNiSn and HfNiSn samples in Fig 2(c), which is consistent with our previous work, demonstrating that even a small amount of intrinsic atomic disorder was sufficient to impose significant influences on the charge transport process.[14] The presence of intrinsic atomic defects in $Zr_{1-x}Hf_xNiSn_{0.985}Sb_{0.015}$ may weaken the potential energy fluctuation by Hf/Zr disorder.

The Seebeck coefficient S exhibits the temperature dependence and sign expected for heavily doped n-type semiconductors, as shown in Fig. 3(a). All the samples have similar Seebeck coefficient values due to the similar carrier concentration in terms of the isoelectronic substitution. The calculated trend of S by SKB model with m^*~2.6 m_e and n_H = 4.0×10^{20} cm^{-3} at 300 K agrees well with the experimental data before the excitation of minority carriers. High power factor ~ 4.5×10^{-3} $Wm^{-1}K^{-2}$ at 800 K was achieved for all the samples through the whole composition range without deterioration.[41]

The measured thermal diffusivities (D) and specific heat (C_p) of all the samples are presented in Fig. 4(a) and Fig. 4(b), respectively. The specific heat increases steadily with temperature. With increasing the Hf content, the C_p at each temperature decreases due to the increased averaged atomic mass. For comparison, the Dulong Petit value of $HfNiSn_{0.985}Sb_{0.015}$ sample is also shown in Fig. 4(b). The thermal conductivity decreases with temperature for all the samples before the bipolar contribution, as shown in Fig. 4(c). The electronic thermal conductivity was calculated by the Wiedemann-Franz law using the calculated Lorenz number by the SKB model.[14,25] Since Hf/Zr alloy hardly affects the electrical properties, the electrical thermal conductivities are very close and thus only one set of κ_e data is shown for clarity. It can be seen in Fig. 4(d) that the κ_L of all the alloyed samples follow a $\kappa_L \sim T^{-0.5}$ relationship before intrinsic excitation, which should be caused by the strong point defect scattering.[41]

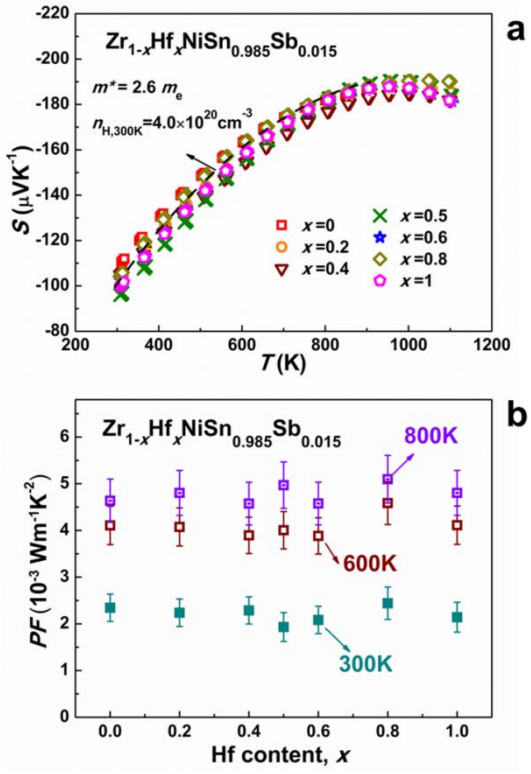

Fig.3 (a) Seebeck coefficient as a function of temperature, and (b) power factor as a function of Hf content for $Zr_{1-x}Hf_xNiSn_{0.985}Sb_{0.015}$ (x = 0 - 1) samples.

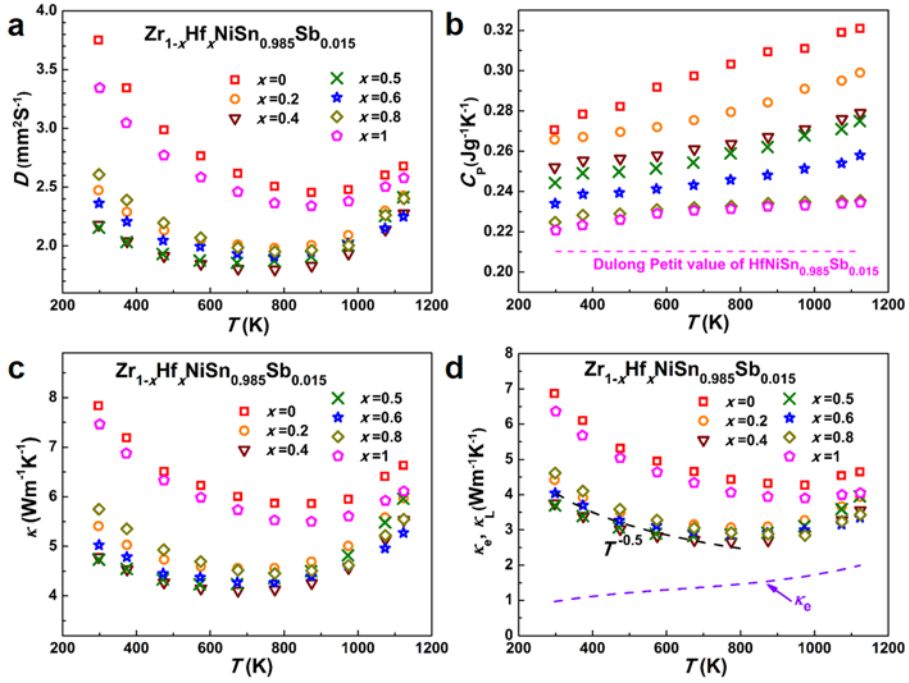

Fig. 4 Temperature dependence of (a) thermal diffusivity, (b) specific heat capacity, (c) thermal conductivity and (d) lattice thermal conductivity and electrical thermal conductivity for $Zr_{1-x}Hf_xNiSn_{0.985}Sb_{0.015}$ (x = 0 - 0.1) samples.

Thermal conductivity is typically limited by phonon-phonon scattering (the Umklapp process), electron-phonon scattering, point defect scattering, and boundary scattering. With the assumption of Matthiessen's rule,[42] the combined relaxation time (τ_C) can be obtained by the addition of the inverse relaxation times for the different scattering process, $\tau_c^{-1} = \sum_i \tau_i^{-1}$, where, τ_i refers to the phonon relaxation time for the *i*th scattering process. The relaxation times, which are functions of frequency and temperature, are calculated (not fitting) here using some characteristic parameters of the HH material, *e.g.*, the Grueneisen parameter and the disorder scattering parameters. Detailed calculation process can be found in our previous work.[13] The scattering mechanisms mentioned above target different populations of phonons. The curves in Fig.5 are calculated at 400 K, when all of the vibration modes have been excited and the maximum phonon frequency is the Debye frequency. Comparing Fig. 5(a) with (b), one can see that the reduction of total effective phonon relaxation time, which arises from the enhancement of point defect scattering by Hf occupying at Zr sites, is the key reason that leads to the decrease of lattice thermal conductivity.

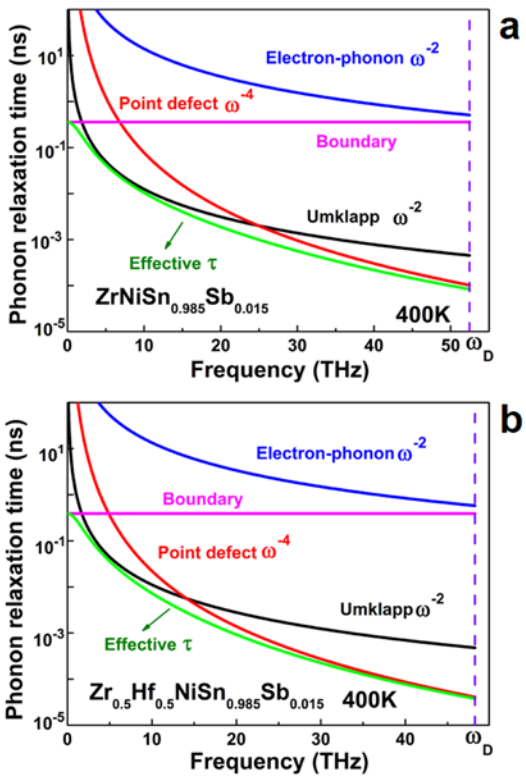

Fig.5 Calculated phonon relaxation time (τ) versus frequency (ω) for $ZrNiSn_{0.985}Sb_{0.015}$ (a) and $Zr_{0.5}Hf_{0.5}NiSn_{0.985}Sb_{0.015}$ (b) samples.

If the scattering from boundaries and electron-phonon is negligible, as the case for *M*NiSn in Fig. 5, the dominant phonon scattering mechanisms in solid solutions would be the Umklapp process and point defect disorders. The ratio of κ_L of the crystal with disorder to that without disorder, κ_L^P, is proposed by Callaway[26] and Klemens[27], and has been successfully used in various alloy systems for thermal conductivity estimation[6,43,44]:

$$\frac{\kappa_L}{\kappa_L^P} = \frac{\tan^{-1}(u)}{u}, \quad u^2 = \frac{\pi^2 \theta_D \Omega}{h v^2} \kappa_L^P \Gamma_{exp} \qquad (1)$$

where *u*, Ω, *h*, *v*, and Γ_{exp} are the disorder scaling parameter, the average volume/atom, the Planck constant, the average sound velocity, and the experimental disorder scattering parameter, respectively. As for κ_L^P, a value of 12.39 $Wm^{-1}K^{-1}$ from a single crystal sample is used for ZrNiSn at 300 K[45]. An approximate $\kappa_L \sim T^{-1}$ relationship is observed in that sample, which indicates that only Umklapp process exists. Taking ZrNiSn as the reference, we can calculate the κ_L^P of HfNiSn using the Callaway model[26], and this yields κ_L^P = 10.90 $Wm^{-1}K^{-1}$ at 300 K. For a specific composition of alloyed sample, the κ_L^P is estimated by taking a weighted average of the lattice thermal conductivities of pure ZrNiSn and HfNiSn.

The Γ_{exp} is assumed to be the sum of the mass fluctuation scattering parameter Γ_M and the strain field fluctuation scattering parameter Γ_S. Yang *et al.* have successfully demonstrated the use of these disorder scattering parameters in ZrNiSn-based HH alloys.[43] In the determination of Γ_S, the only adjustable patameter ε, which normally ranges from 10 to 100, is given by,[46]

$$\varepsilon = \frac{2}{9}\left(\frac{6.4 \times \gamma(1+\upsilon_P)}{(1-\upsilon_P)}\right)^2 \qquad (2)$$

where γ and υ_P are the Grueneisen parameter and Poisson ratio, respectively. They can be calculated on the basis of the sound velocity measurement. Since Sb has the similar atomic radius and mass to Sn and the Sb content is small, the effect of disorder on the Sn sublattice is neglected. Thus, the disorder scattering parameter Γ_{vacant} arising from intrinsic Ni-interstitial atomic disorder can be deduced from the measured κ_L of $ZrNiSn_{0.985}Sb_{0.015}$ and $HfNiSn_{0.985}Sb_{0.015}$ by Eq. 1, and Γ_{vacant}=0.0397 and 0.0288 are obtained respectively. The small difference between these two values may be attributed mostly to the different average mass of the compounds. Assuming the amount of intrinsic disorders in different samples are mostly the same, we can thus get Γ_{total} by integration of the calculated $\Gamma_{Hf/Zr}$ and experimentally determined Γ_{vacant}. The obtained Γ_{total}, $\Gamma_{Hf/Zr}$, and ε are listed in Table 1.

Table 1 Disorder parameters from mass and strain for *M*NiSn

Samples	$\Gamma_{Hf/Zr}$		Γ_{total}	ε
	Γ_M	Γ_S		
$ZrNiSn_{0.985}Sb_{0.015}$	...	...	0.0397	38.9
$Zr_{0.8}Hf_{0.2}NiSn_{0.985}Sb_{0.015}$	0.0583	0.0023	0.1050	54.3
$Zr_{0.6}Hf_{0.4}NiSn_{0.985}Sb_{0.015}$	0.0778	0.0046	0.1249	61.7
$Zr_{0.5}Hf_{0.5}NiSn_{0.985}Sb_{0.015}$	0.0766	0.0033	0.1075	39.1
$Zr_{0.4}Hf_{0.6}NiSn_{0.985}Sb_{0.015}$	0.0697	0.0054	0.1123	61.7
$Zr_{0.2}Hf_{0.8}NiSn_{0.985}Sb_{0.015}$	0.0418	0.0032	0.0731	48.8
$HfNiSn_{0.985}Sb_{0.015}$	...	...	0.0288	52.3

Fig. 6 shows the lattice thermal conductivity at 300 K and 600 K as a function of solid solution composition. The solid curves were calculated by Eq. 1. The experimental results, together with the literature data[16,24,47,48], agree well with the theoretical curves. The relative reduction of κ_L compared to un-alloyed ZrNiSn or HfNiSn decreases with temperature rising from 300 K to 600 K. The 20% Hf substitution in ZrNiSn causes about 40% reduction in κ_L at 300 K, while the same amount of Zr at HfNiSn causes about 20% reduction in κ_L. And the κ_L reduction by further substitution becomes relatively small in the range of x = 0.2 - 0.8.

The temperature dependence of figure of merit zT is shown in Figure 7. All the substituted samples exhibit improved zTs, compared to the parent compounds of ZrNiSn and HfNiSn at different temperatures, implying that the alloy disorder is beneficial for enhancing TE performance of the HH alloys due to the reduced lattice thermal conductivity. The highest zT value reaches ~1.1 at 1000 K for $Hf_{0.8}Zr_{0.2}NiSn_{0.985}Sb_{0.015}$, better than the traditional SiGe alloys (peak zT ~ 0.6), demonstrating the promise for high temperature applications. In fact, the HH alloys have also lower cost than SiGe alloy. In addition, the mechanical robustness and thermal stability of these alloys are really better than many other thermoelectric materials, which will also be beneficial for the large-scale commercialization.

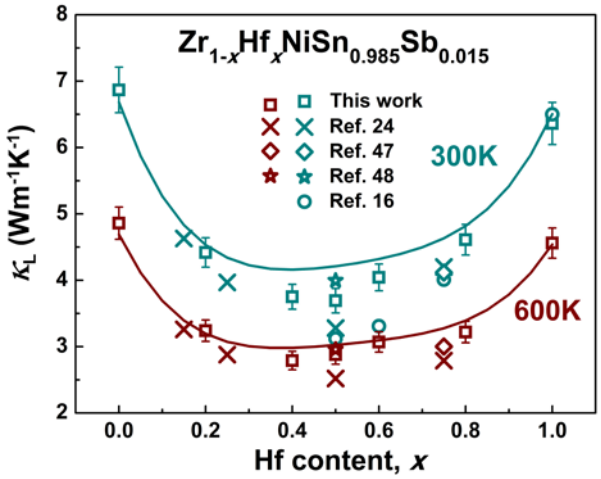

Fig.6 Lattice thermal conductivity at 300 K and 600 K as a function of Hf content. The solid curves were calculated from the model described by Eq. 1.

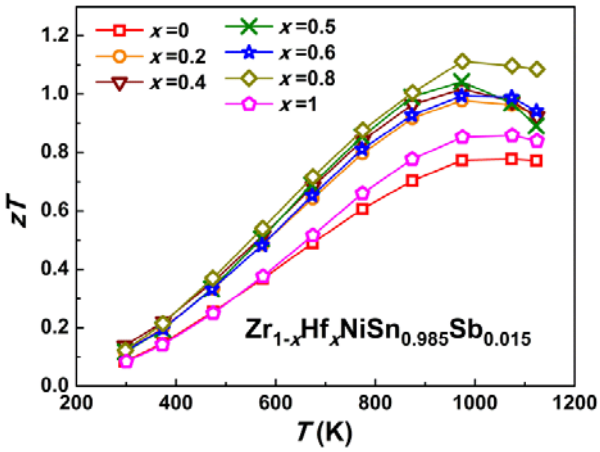

Fig.7 Temperature dependence of the dimensionless figure of merit zT for $Zr_{1-x}Hf_xNiSn_{0.985}Sb_{0.015}$ (x = 0 - 0.1) samples

Conclusions

Isoelectronic alloying of Hf was introduced to the intrinsically disordered ZrNiSn HH system. The point defect disorder of Zr/Hf atoms in *M*NiSn (*M* = Hf, Zr, Ti) HH alloys effectively reduces lattice thermal conductivity as predicted from point defect scattering. However the introduced local atomic disorder produces negligible effect on the electron scattering process and the conduction band structure. The electron alloy scattering potential observed on the conduction band electrons is less than 0.1 eV, ten times less than typically observed. This phenomenon can be understood from the existence of intrinsic atomic disorder in *M*NiSn system that effectively screens the effect of the induced disorder by Hf/Zr. The highest $zT \approx 1.1$ was obtained for $Zr_{0.2}Hf_{0.8}NiSn_{0.985}Sb_{0.015}$ at 1000 K. This results in a substantial improvement in zT due to alloying on the Zr/Hf site that doesn't require nanoscale microstructures to avoid scattering of charge carriers. Based on our encouraging results, further suppression of lattice thermal conductivity by multi-component alloying is possible, and further research should be focused on reducing the amount of Hf usage in consideration of cost.

Acknowledgments

The work was supported by the National Basic Research Program of China (2013CB632503), the Nature Science Foundation of China (51171171), the Program for New Century Excellent Talents in University (NCET-12-0495), the Program for Innovative Research Team in University of Ministry of Education of China (IRT13037), and EFRC Solid-State Solar-Thermal Energy Conversion Center (S3TEC) award number DE-SC0001299.

Reference

1 T. M. Tritt, *Science*, 1999, **283**, 804-805.
2 R. Chasmar and R. Stratton, *J. Electron. Control.*, 1959, **7**, 52-72.

3 Y. Z. Pei, A. D. LaLonde, H. Wang and G. J. Snyder, *Energy Environ. Sci.*, 2012, **5**, 7963-7969.
4 G. A. Slack, in *CRC Handbook of Thermoelectrics*, ed. D. M. Rowe, CRC Press, Boca Raton, 1995, p. 407.
5 X. H. Liu, T. J. Zhu, H. Wang, L. P. Hu, H. H. Xie, G. Y. Jiang, G. J. Snyder and X. B. Zhao, *Adv. Energy Mater.*, 2013, **3**, 1238-1244.
6 H. Wang, A. D. LaLonde, Y. Z. Pei and G. J. Snyder, *Adv. Funct. Mater.*, 2013, **23**, 1586-1596.
7 S. N. Girard, T. C. Chasapis, J. Q. He, X. Y. Zhou, E. Hatzikraniotis, C. Uher, K. M. Paraskevopoulos, V. P. Dravid and M. G. Kanatzidis, *Energy Environ. Sci.*, 2012, **5**, 8716-8725.
8 L. D. Zhao, H. J. Wu, S. Q. Hao, C. I. Wu, X. Y. Zhou, K. Biswas, J. Q. He, T. P. Hogan, C. Uher, C. Wolverton, V. P. Dravid and M. G. Kanatzidis, *Energy Environ. Sci.*, 2013, **6**, 3346-3355.
9 S. R. Culp, J. Simonson, S. J. Poon, V. Ponnambalam, J. Edwards and T. M. Tritt, *Appl. Phys. Lett.*, 2008, **93**, 022105.
10 J. Yang, H. M. Li, T. Wu, W. Q. Zhang, L. D. Chen and J. H. Yang, *Adv. Funct. Mater.*, 2008, **18**, 2880-2888.
11 C. G. Fu, T. J. Zhu, Y. Z. Pei, H. H Xie, H. Wang, G. J. Snyder, Y. Liu, Y. T. Liu and X. B. Zhao, *Adv. Energy Mater.*, 2014, **4**, 1400600.
12 C. G. Fu, T. J. Zhu, Y. T Liu, H. H Xie and X. B. Zhao, *Energy Environ. Sci.*, 2015, **8**, 216-220.
13 H. H. Xie, H. Wang, Y. Z. Pei, C. G. Fu, X. H. Liu, G. J. Snyder, X. B. Zhao and T. J. Zhu, *Adv. Funct. Mater.*, 2013, **23**, 5123-5130.
14 H. H. Xie, H. Wang, C. G. Fu, Y. T. Liu, G. J. Snyder, X. B. Zhao and T. J. Zhu, *Sci. Rep.*, 2014, **4**, 6888.
15 C. Uher, J. Yang, S. Hu, D. T. Morelli and G. P. Meisner, *Phys. Rev. B*, 1999, **59**, 8615-8621.
16 C. Yu, T. J. Zhu, R. Z. Shi, Y. Zhang, X. B. Zhao and J. He, *Acta Mater.*, 2009, **57**, 2757-2764.
17 P. F. Qiu, J. Yang, X. Y. Huang, X. H. Chen and L. D. Chen, *Appl. Phys. Lett.*, 2010, **96**, 152105.
18 T. Harman, P. Taylor, M. Walsh and B. LaForge, *Science*, 2002, **297**, 2229-2232.
19 L. D. Chen, X. Y. Huang, M. Zhou, X. Shi and W. B. Zhang, *J. Appl. Phys.*, 2006, **99**, 064305.
20 X. Yan, W. S. Liu, S. Chen, H. Wang, Q. Zhang, G. Chen and Z. F. Ren, *Adv. Energy Mater.*, 2013, **3**, 1195-1200.
21 G. Joshi, X. Yan, H. Z. Wang, W. S. Liu, G. Chen and Z. F. Ren, *Adv. Energy Mater.*, 2011, **1**, 643-647.
22 H. H. Xie, C. Yu, T. J. Zhu, C. G. Fu, G. J. Snyder and X. B. Zhao, *Appl. Phys. Lett.*, 2012, **100**, 254104.
23 C. Yu, H. H. Xie, C. G. Fu, T. J. Zhu and X. B. Zhao, *J. Mater. Res.*, 2012, **27**, 2457-2465.
24 S. Chen, K. C. Lukas, W. S. Liu, C. P. Opeil, G. Chen and Z. F. Ren, *Adv. Energy Mater.*, 2013, **3**, 1210-1214.
25 H. Wang, Y. Z. Pei, A. D. LaLonde and G. J. Snyder, *Proc. Natl. Acad. Sci. U.S.A.*, 2012, **109**, 9705-9709.
26 J. Callaway and H. C. von Baeyer, *Phys. Rev.*, 1960, **120**, 1149-1154.
27 P. Klemens, *Phys. Rev.*, 1960, **119**, 507.
28 K. A. Borup, E. S. Toberer, L. D. Zoltan, G. Nakatsukasa, M. Errico, J. P. Fleurial, B. B. Iversen and G. J. Snyder, *Rev. Sci. Instrum.*, 2012, **83**, 123902.
29 S. Ögüt and K. M. Rabe, *Phys. Rev. B*, 1995, **51**, 10443-10453.
30 P. Larson, S. D. Mahanti and M. G. Kanatzidis, *Phys. Rev. B*, 2000, **62**, 12754-12762.
31 L. Chaput, J. Tobola, P. Pécheur and H. Scherrer, *Phys. Rev. B*, 2006, **73**, 045121.
32 P. Larson, S. D. Mahanti, S. Sportouch and M. G. Kanatzidis, *Phys. Rev. B*, 1999, **59**, 15660-15668.
33 C. Yu, T. J. Zhu, K. Xiao, J. J. Shen, S. H. Yang and X. B. Zhao, *J. Electron. Mater.*, 2010, **39**, 2008-2012.
34 V. W. L. Chin, R. J. Egan and T. L. Tansley, *J. Appl. Phys.*, 1991, **69**, 3571-3577.
35 S. Krishnamurthy, A. Sher and A. B. Chen, *Appl. Phys. Lett.*, 1985, **47**, 160-162.
36 T. J. Zhu, H. L. Gao, Y. Chen and X. B. Zhao, *J. Mater. Chem. A*, 2014, **2**, 3251-3256.
37 H. H. Xie, J. L. Mi, L. P. Hu, N. Lock, M. Chirstensen, C. G. Fu, B. B. Iversen, X. B. Zhao and T. J. Zhu, *CrystEngComm*, 2012, **14**, 4467-4471.
38 F. Aliev, N. Brandt, V. Kozyr'kov, V. Moshchalkov, R. Skolozdra, V. Stadnyk Yu and V. Pecharskii, *JETP Lett.*, 1987, **45**, 684-686.
39 K. Miyamoto, A. Kimura, K. Sakamoto, M. Ye, Y. Cui, K. Shimada, H. Namatame, M. Taniguchi, S. I. Fujimori and Y. Saitoh, *Appl. Phys. Express*, 2008, **1**, 081901.
40 V. Romaka, P. Rogl, L. Romaka, Y. Stadnyk, A. Grytsiv, O. Lakh and V. Krayovskii, *Intermetallics*, 2013, **35**, 45-52.
41 T. J. Zhu, C. G. Fu, H. H. Xie, Y. T. Liu and X. B. Zhao, *Adv. Energy Mater.*, 2015, **5**, 1500588
42 N. W. Ashcroft and N. D. Mermin, *Solid State Physics*, Thomson Learning, New York, 1976.
43 J. Yang, G. Meisner and L. Chen, *Appl. Phys. Lett.*, 2004, **85**, 1140-1142.
44 B. Abeles, *Phys. Rev.*, 1963, **131**, 1906-1911.
45 W.kaefer, K, Fess, Ch. Kloc, K. Friemelt, and E.Bucher, Proceedings of the 16th International Conference on Thermoelectrics, Dresden, 1997.
46 C. L. Wan, W. Pan, Q. Xu, Y. X. Qin, J. D. Wang, Z. X. Qu, and M. H. Fang, *Phys. Rev. B,* 2006, **74**, 144109.
47 S. R. Culp, S. J. Poon, N. Hickman, T. M. Tritt and J. Blumm, *Appl. Phys. Lett.*, 2006, **88**. 042106.
48 S. Sakurada and N. Shutoh, *Appl. Phys. Lett.*, 2005, **86**. 082105.